Mechanism of single-bubble sonoluminescence

Yu An

Physics Department, Tsinghua University, Beijing 100084 and Institute of Acoustics, Chinese Academy of Science, Beijing 100080
(Received 8 January 2006; revised manuscript received 25 April 2006; published 21 August 2006)

Considering almost all the effective processes of physics and chemical reaction in our numerical computation model, we investigate the mechanism of single bubble sonoluminescence (SBSL). For those sonoluminescing single bubbles in water at its flashing phase, the numerical simulation reveals that if the temperature inside the bubble is not high enough which may result in the plenty oxygen molecules and OH radicals undissociated, such as the case of a single argon bubble in 20 °C or 34 °C water, the radiative attachment of electrons to oxygen molecules and OH radicals contributes most to the SBSL; if the temperature inside the bubble is higher which makes most of the water vapor inside the bubble dissociate into oxygen and hydrogen atoms, such as the case of an argon bubble or a helium bubble in 0 °C water, the radiative attachment of electrons to oxygen and hydrogen atoms dominates the SBSL; if the temperature is still higher, such as the case of a xenon bubble in 0 °C water, the contribution from electron-neutral atom bremsstrahlung and electron-ion bremsstrahlung and recombination would be comparable with the contribution from the radiative attachment of electrons to oxygen and hydrogen atoms, and they together dominate the SBSL. For sonoluminescing single bubbles in those low vapor pressure liquids, such as in 85 wt. % sulphuric acid, the electron-neutral atom bremsstrahlung and the electron-ion bremsstrahlung and recombination contribute most to the continuous spectrum part of SBSL. The present calculation also provides good interpretations to those observed phenomena, such as emitted photon numbers, the width of optical pulses, the blackbody radiation like spectra. The temperature fitted by the blackbody radiation formula is very different from that calculated by the gas dynamics equations. Besides, the effect of chemical dissociation on the shock wave is also discussed.

INTRODUCTION

A single oscillating gas bubble can be trapped at the velocity node of an acoustic standing wave in water. A fascinating accompanying phenomenon is the periodic emission by the bubble of very short light pulses in harmony with the oscillation of the acoustic field, known as single bubble sonoluminescence or SBSL [1,2]. Some typical characters of SBSL observed in experiments are: (a) in every period the emitted photon number is about 10^4–10^6, in 85 wt. % sulphuric acid the emitted photon number of SBSL may be larger [3]; (b) the full width at half maximum (FWHM) of the optical pulses is in the range of 40–300 ps [4] and it is, for most of the cases of a single argon bubble, independent of wavelength [5], an exception is also observed [6]; (c) the light intensity is sensitive to the ambient temperature [7]; (d) the light spectra are continuous and most of them are well fitted by the blackbody radiation formula [8,9], under specific conditions the line spectrum of OH radical [10] and Ar atom [3] can be seen occasionally. The wavelength independence of FWHM excludes the mechanism of thermal radiation [11]. Thus another mechanism of the light emission with the continuous spectrum connecting to high temperature is brought to prominence. It is the bremsstrahlung and recombination radiation [12] that makes it possible for the wavelength independence of FWHM of a sonoluminescing argon bubble to be well interpreted, but the problem is that the vapor effect is excluded in that calculation [12]. In fact, water vapor inside the bubble plays an important role in SBSL [13]. For example, it greatly lowers the maximum temperature in the bubble [14,15] due to its large heat capacity and the occurrence of endothermic chemical dissociation. The

character (c) mentioned above is just the result of the water vapor effect that water vapor pressure is sensitive to temperature. If the water vapor is considered in the calculation, the maximum temperature inside the bubble seems to be too low [16–19] to emit enough photons as measured in experiments. On the contrary, the other calculations with the bremsstrahlung and recombination radiation model and the radiative attachment of electrons to atoms seem to well reproduce the experimental data of emitted photon numbers of SBSL [20,21]. We find that this controversy is originated from different employment of the gas dynamics. [20,21] employ the so-called uniform model, in which the water vapor effect is included, but the important process that the diffusion between the water vapor and the inert gas is omitted in the calculation which leads to very small amount of residual water vapor remaining and much higher temperature achieving in the bubble when the bubble is at its flashing phase, and the contribution from the radiative attachment of electrons to atoms is just a compensation to the bremsstrahlung and recombination radiation model.

Besides the photon number, there are other experimental results, such as the spectrum and the pulse width, which need to be interpreted too. In the recent paper [22], the gas dynamics model with the partial differential equations of fluid mechanics and various processes, such as heat transmission, viscous dissipation, mass diffusion, the phase transition of water vapor at interface, is propounded, in which the calculated FWHM's of SBSL with the bremsstrahlung and recombination radiation model are in ~100 ps. However, the results could not be compared directly with the experimental data, because the chemical reactions were excluded in that calculation. In the present paper, we will consider the chemical dissociation reaction by the so-called law of mass action

026304-1

for chemical equilibrium [23]. Then, the bremsstrahlung and recombination radiation together with the radiative attachment of electrons to oxygen and hydrogen atoms and to oxygen molecules and OH radicals can be employed to evaluate the light emission. In fact, these processes are the most reasonable candidates of the mechanisms of SBSL for those high temperature gases emitting the continuous spectrum.

This paper is organized as follows: First, the computation model and the formulation are provided. Next, the emitted photon numbers of SBSL is calculated and the contributions from the different mechanisms are compared with the experimental data. Then, the change of the contents in the bubble due to the chemical reaction and the ionization is calculated; after a brief discussion of the validity of the assumption of the chemical equilibrium in the present model I will show the calculated results about the distribution of the absorption coefficients of the different mechanisms in the bubble, the optical pulses, the spectra and their best fit to the black body radiation; then the effect of chemical reaction on the shock wave is discussed. In addition, the case of SBSL in 85 wt. % sulphuric acid is calculated. Finally, a conclusion will be made.

COMPUTATION MODEL AND FORMULATION

Gas dynamics and chemical reaction

As argued in [22], the choice of the different RP equation forms [24] and the adoption of the different values of the accommodation coefficient of water vapor would strongly affect the final calculation. It happens that the accommodation coefficient of water vapor is evaluated by the molecular dynamics model [25], recently. We rationally adopt this calculated result in the present paper. The problem is the RP equation, in a rigorous sense, the accurate equation of the bubble wall motion is unknown yet, therefore, we have to steer clear of this problem and simply choose the earlier form of the RP equation [24] in the calculation. This RP equation is as follows:

$$R\ddot{R} + \frac{3}{2}\dot{R}^2 = \frac{1}{\rho_{l\infty}}[p_l - p_\infty - p_s(t + t_R)] + \frac{t_R}{\rho_{l\infty}}\dot{p}_l, \qquad (1)$$

where $R(t)$ is the radius of the bubble, $\rho_{l\infty}$ the ambient liquid density, p_∞ the ambient pressure, $p_s(t) = -p_a \sin(\omega t)$ the driving acoustic pressure, $t_R \equiv R/c_{l\infty}$, $c_{l\infty}$ the sound speed in the liquid at the ambient temperature and pressure of 1 atm, $p_l = p_g(R,t) - 4\eta\dot{R}/R - 2\sigma/R$ the pressure on the liquid side of the bubble wall, $p_g(R,t)$ the pressure on the gas side of the bubble wall, η the dynamic viscosity, σ the surface tension coefficient of the liquid. The RP equation should be in conjunction with the gas dynamics equations inside the bubble.

In the case of SBSL, only the inert gases and the vapor of surrounding liquid can fill the bubble due to the effect of the inert gas rectification [26]. As we know the duration of the bubble collapse phase is very short and the chemical dissociation mainly takes place in this period. Therefore, in the present model, as an approximation we will neglect the diffusion of those chemical dissociation products and consider only the partial differential equations (PDE) of fluid mechan-

ics of two kinds of gas component, the inert gas and the water vapor. The validity of this approximation will be discussed later. The PDE in spherical symmetry takes the following form:

$$\frac{\partial \rho_1}{\partial t} + \frac{1}{r^2}\frac{\partial}{\partial r}[r^2(\rho_1 v + J_1)] = 0,$$

$$\frac{\partial \rho}{\partial t} + \frac{1}{r^2}\frac{\partial}{\partial r}(r^2 \rho v) = 0,$$

$$\frac{\partial(\rho v)}{\partial t} + \frac{1}{r^2}\frac{\partial}{\partial r}(r^2 \rho v^2) + \frac{\partial p}{\partial r} = \frac{1}{r^2}\frac{\partial}{\partial r}(r^2 \tau_{rr}) + \frac{\tau_{rr}}{r},$$

$$\frac{\partial E}{\partial t} + \frac{1}{r^2}\frac{\partial}{\partial r}\{r^2[(E+p)v + q]\} = \frac{1}{r^2}\frac{\partial}{\partial r}(r^2 v \tau_{rr}), \qquad (2)$$

where t is the time, r the radial coordinate, ρ_i the density of the ith gas, and $\rho = \rho_1 + \rho_2$ the density of the gas mixture, v_i the radial component of the ith gas velocity, v the average velocity, $\rho v = \rho_1 v_1 + \rho_2 v_2$, p the gas pressure, q the heat flux, J_1 the diffusion mass flux of species 1 (the vapor) with respect to the average velocity, $J_1 = \rho_1(v_1 - v)$, $\tau_{rr} = (4\mu/3) \times (\partial v/\partial r - v/r)$, μ is the dynamic viscosity, $E = E_1 + E_2$ the total energy density, $E_i = \rho_i v_i^2/2 + \rho_i e_i$, e_i is the internal energy of the ith gas.

In the present model, the chemical equilibrium is assumed at any time and any local in the bubble, once the pressure and the temperature are given, the chemical dissociation products, such as oxygen and hydrogen atoms, OH radicals etc., and those ionized positive and negative ions and electrons can be evaluated immediately by the law of mass action. As to the validity of the application of this law to the present calculation, we will discuss it in the next section. The chemical dissociation reactions we take into account in the present model are

$$H_2O \leftrightarrow OH + H, \qquad (3)$$

$$OH \leftrightarrow O + H, \qquad (4)$$

$$O + O \leftrightarrow O_2, \qquad (5)$$

$$H + H \leftrightarrow H_2, \qquad (6)$$

and ionization processes

$$M \leftrightarrow M^+ + e, \qquad (7)$$

where M denotes Ar and those atoms and molecules appearing in (3)–(6), and the processes of the attachment of electrons to hydrogen and oxygen atoms or related molecules

$$M + e \leftrightarrow M^-, \qquad (8)$$

where M^- denotes negative ions O^-, H^-, O_2^-, OH^-. By the law of mass action, we can evaluate the number density of the products of the chemical dissociation and the ionized electrons, as well as the positive and the negative ions. The formulas are sketched in Appendix A.

In this case, the contributions of those chemical dissociation and ionization energies, and those dissociated and ionized products should be included in the internal energy term, and if one rewrites the total energy density of the gas mixture as $E = \rho v^2/2 + S$, then

$$S = \frac{1}{2}\left(\frac{1}{\rho_1} + \frac{1}{\rho_2}\right)J_1^2 + \sum_i \nu_i^+ \varepsilon_i^+ + \sum_j \xi_j \varepsilon_j - \sum_i \nu_i^- \varepsilon_i^-$$

$$+ \left[\frac{3}{2}\nu_{\text{mono}} + \nu_{\text{H}_2\text{O}}\left(3 + \sum_{i=1}^3 \frac{\theta_i/T}{\exp(\theta_i/T) - 1}\right) + \sum_k \bar{\nu}_k\left(\frac{5}{2}\right.\right.$$

$$\left.\left.+ \frac{\bar{\theta}_k/T}{\exp(\bar{\theta}_k/T) - 1}\right)\right]\tilde{R}T \tag{9a}$$

with

$$\xi_{\text{H}_2\text{O}} = \nu_1 - \nu_{\text{H}_2\text{O}} - \nu_{\text{H}_2\text{O}}^+,$$

$$\xi_{\text{OH}} = \xi_{\text{H}_2\text{O}} - \nu_{\text{OH}} - \nu_{\text{OH}}^+,$$

$$\xi_{\text{O}_2} = (\nu_{\text{O}} + \nu_{\text{O}}^+ + \nu_{\text{O}}^- - \xi_{\text{OH}})/2,$$

$$\xi_{\text{H}_2} = (\nu_{\text{H}} + \nu_{\text{H}}^+ + \nu_{\text{H}}^- - \xi_{\text{H}_2\text{O}} - \xi_{\text{OH}})/2, \tag{9b}$$

where ν_i^+ is the mole density of the ith positive ion, ε_i^+ the mole ionization energy of the ith molecule or atom, ε_j the mole dissociation energy of $j = \text{H}_2\text{O}$, OH, O_2, H_2, respectively, ν_i^- the mole density of O^-, H^-, O_2^-, OH^-, and ε_i^- their mole electron affinity, ν_{mono} the mole density of the total monoatoms, ν_1 the mole density of the vapor when the chemical reaction is ignored, ν_i the mole density of the i atom or molecule, $\bar{\nu}_k$ the mole density of OH, O_2, H_2, respectively, $\tilde{R} = 8.31$ J/(mol K) the gas constant, T the temperature, θ_i three vibration energies of water molecule, $\bar{\theta}_k$ the vibration energy of OH, O_2, H_2 respectively. From Eqs. (9a) and (9b), we can reevaluate the temperature correcting for the effects of the chemical dissociation processes.

Besides, the van der Waals form of the equation of state of the gases inside the bubble is adjusted as

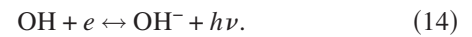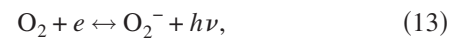$$p = \frac{\tilde{\nu}\tilde{R}T}{1 - \sum_i \nu_i b_i} - \nu^2 a, \tag{10}$$

where $\tilde{\nu}$ is the mole density of the total particles, a is the parameter of the van der Waals equation, and $\nu = \nu_{\text{Ar}} + \nu_1$. For simplicity, regardless with or without considering the chemical dissociation, both ν and a take the same. Another approximation we take in the calculation is that for those O atoms, and H_2O, OH, O_2 and their negative and positive ions, the van der Waals hard core volume is equally taken as $b_{\text{H}_2\text{O}} = 3.07 \times 10^{-5}$ m³/mol, while for those hydrogen atoms and molecules, and their negative and positive ions, the van der Waals hard core volume is equally taken as $b_{\text{H}_2} = 2.65 \times 10^{-5}$ m³/mol. The other equations and formulas, such as heat conductivity, viscosity, diffusion of mass, energy balance equation in the surrounding liquid, the phase transition

of water vapor at the interface and boundary conditions, etc. are exactly the same as those listed in [22].

Radiation model

The formulas of absorption coefficient of electron-ion bremsstrahlung and recombination radiation (EIBR) are exactly the same as those listed in the supplement of [12]. The tabulated absorption coefficients of electron-neutral atom bremsstrahlung (EAB)[27] are referenced and extrapolated to the higher temperature case. The extrapolating formulas of Ar, He, Xe, O, H atoms are sketched in Appendix B. The processes of the radiative attachment of electrons to atoms (RAEA) or to molecules (RAEM) are

$$\text{O} + e \leftrightarrow \text{O}^- + h\nu, \tag{11}$$

$$\text{H} + e \leftrightarrow \text{H}^- + h\nu, \tag{12}$$

$$\text{O}_2 + e \leftrightarrow \text{O}_2^- + h\nu, \tag{13}$$

$$\text{OH} + e \leftrightarrow \text{OH}^- + h\nu. \tag{14}$$

The analytic fit formula of absorption cross section of O^-[28] as a function of the photon energy is referenced from [21], and the tabulated absorption cross section of H^-[29] as a function of the photon wavelength is from [30]. In Appendix B, we deliver the analytic fit formulas of the absorption cross section of OH^-[31] and O_2^- [32] as a function of the photon wavelength and the photon energy, respectively. The effective absorption coefficient can then be calculated. Once the coefficient of absorption κ is obtained, the radiation intensity, watt per unit wavelength interval, solid angle, and projected surface area, that has traveled a distance s through a bubble (radius R) can be evaluated as follows:

$$I_\lambda(s,t) = \int_0^s n^2 \kappa P_\lambda^{\text{Pl}} e^{-\kappa x} dx, \tag{15}$$

where P_λ^{Pl} is the Planck radiation intensity, n the indices of refraction which is almost unity. Then the total emitted power from the bubble per wavelength interval at wavelength λ is

$$P_\lambda(t) = 8\pi^2 \int_0^R I_\lambda(s,t)y\,dy, \tag{16}$$

where $s = 2\sqrt{R^2 - y^2}$.

RESULTS AND DISCUSSION

In the previous work [17,18], it is shown that the bremsstrahlung and recombination model alone is insufficient to produce enough photons that are consistent with the experimental results. In the present work, our calculation confirms the previous results and further indicates that it is the radiative attachment of electrons to oxygen and hydrogen atoms or to oxygen and OH molecules that plays an important role in SBSL in water. For SBSL in low vapor pressure liquid, such as in 85 wt. % sulphuric acid, the calculation shows that

TABLE I. Comparison of calculated emitted photon numbers of SBSL in water and experimental data, and corresponding parameters. Where $N_p^{\text{EIBR+EAB}}$ denotes the calculated photon number by the bremsstrahlung and recombination model, N_p^{RAEA} the calculated photon number by the radiative attachment of electrons to oxygen and hydrogen atoms, N_p^{RAEM} the calculated photon number by the radiative attachment of electrons to oxygen and OH molecules, N_p^{exp} the observed photon number [13].

Gases	Ar	Ar	Ar	He	Xe
$T_0(^\circ\text{C})$	0	20	34	0	0
$R_0(\mu\text{m})$	4.55	4.55	4.55	4.55	4.55
$R_m(\mu\text{m})$	37.2	37.2	37.4	37.3	37.1
$p_a(\text{atm})$	1.35	1.34	1.31	1.35	1.35
$f(\text{kHz})$	31.9	33.8	34.3	31.9	31.9
$N_p^{\text{EIBR+EAB}}$	1.13×10^5	3.68×10^3	1.36×10^2	1.03×10^3	1.76×10^6
$N_p^{\text{EIBR+EAB}}+N_p^{\text{RAEA}}$	4.98×10^5	2.55×10^4	4.76×10^2	9.38×10^3	3.40×10^6
$N_p^{\text{EIBR+EAB}}+N_p^{\text{RAEA}}+N_p^{\text{RAEM}}$	5.22×10^5	6.45×10^4	6.15×10^3	1.01×10^4	3.36×10^6
N_p^{exp}	6.0×10^5	6.0×10^4	1.2×10^4	—	—

the bremsstrahlung (electron-neutral atom, electron-ion) and recombination dominate the SBSL.

Photon numbers from different mechanisms

We choose the parameters which appear in [13] to calculate the emitted photon numbers of SBSL, these numerical results are displayed in Table I. We find the contribution of the radiative attachment is really important: for an Ar bubble in 34 °C water, the radiative attachment of electrons to oxygen molecules and OH radicals (RAEM) dominates the SBSL; for an Ar bubble in 20 °C water, the contribution of the radiative attachment of electrons to oxygen and hydrogen atoms (RAEA) is about half of the contribution of RAEM and they together dominate the SBSL; for an Ar or a He bubble in 0 °C water, most of the contribution is from RAEA; for a Xe bubble in 0 °C water, the contributions from the electron-neutral atom bremsstrahlung (EAB) and the electron-ion bremsstrahlung and recombination (EIBR) are close to the contribution from RAEA, and these mechanisms contribute most to the SBSL. The calculated optical pulses may show these arguments more clearly, see Fig. 1.

One may notice that the calculated total photon numbers for an Ar bubble in 0 °C or 20 °C water are consistent with the experimental data, while for an Ar bubble in 34 °C water, it is about half of the observed data. This is acceptable, the reason is as follows. As we know the temperature inside the bubble is very sensitive to residual amount of water vapor in the bubble, and in 34 °C water the vapor pressure is relatively high, thus small changes of some parameters, such

as the binary diffusion coefficient of water vapor on the inert gas, would largely affect the residual amount of water vapor in the bubble. For example, we simply increase 30% of the binary diffusion coefficient, then for 34 °C water, the calculated photon number of SBSL emitted from an argon bubble per flash increases to 1.81×10^4 (it was 6.15×10^3 and the experimental result is 1.2×10^4, see Table I). The binary diffusion coefficient of water vapor on the inert gas is formulated from the empirical molecular theory, according to which in the circumstance of SBSL with high temperature and high pressure, less than 30% error of the binary diffusion coefficient may be acceptable. On the other hand, through the small adjustment of this coefficient or other parameters, it is possible to adjust our calculated results to approach the experimental data.

Chemical dissociation and temperature

In a certain condition, the amount of photon calculated from different radiation mechanisms depends on the temperature and the gas contents inside the bubble, namely the amount of the residual water vapor and its chemical products. Usually, there is a close relationship between the temperature and the gas contents. As a sonoluminescing bubble is expanding or is slowly compressing, the temperature inside the bubble keeps the same as surrounding water, and when the bubble reaches violent collapse phase, the temperature inside the bubble increases dramatically and the chemical dissociation of water vapor occurs. As an example, we perform the numerical simulation of the processes to see how
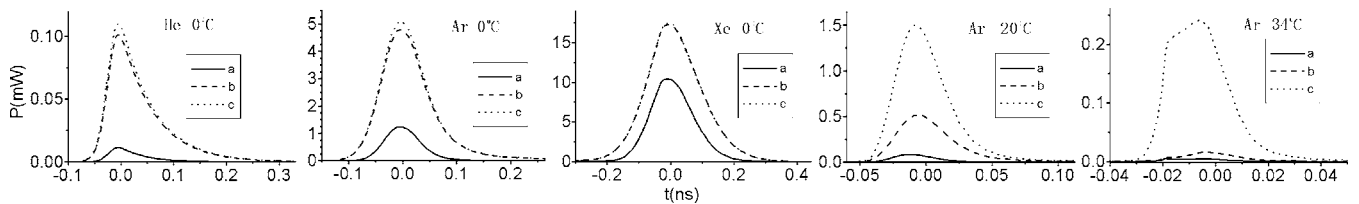

FIG. 1. Optical pulses of SBSL of the different bubbles. Label a, b, c denote the contribution from EIBR+EAB, EIBR+EAB+RAEA, EIBR+EAB+RAEA+RAEM, respectively.
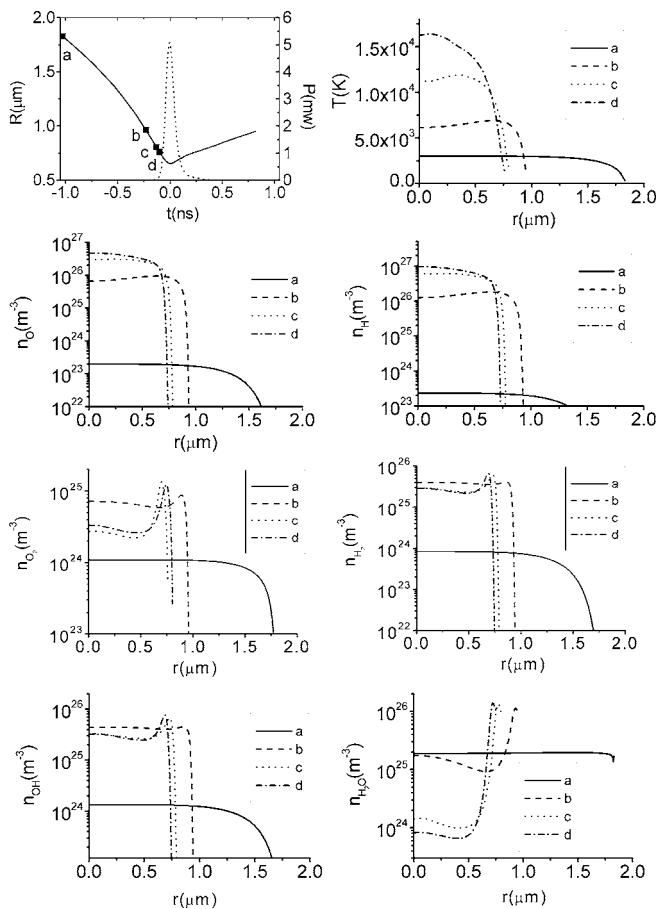
FIG. 2. Radius of an argon bubble $R(t)$ (solid line in the first graph) and the optical pulse of sonoluminescence vs time t (dotted line in the first graph), and spatial profiles of the calculated temperature and number densities of various particles, H_2O, OH, O_2, H_2, O, and H, at the given points of a, b, c, and d (filled squares in the first graph). The ambient temperature $T_0=0$ °C, and the other parameters are the same as those listed in Table I. $t=0$ is set when $R=R_{min}$.

the chemical dissociation changes the gas contents, namely the number density of particles, inside a collapsing Ar bubble in 0 °C water (parameters see Table I), as illustrated in Fig. 2. The first graph in Fig. 2 shows the bubble radius $R(t)$ vs the time (solid line). $t=0$ is set when the bubble is at its minimum size, and the points a, b, c, and d are selected to show the changes. At the same graph, the optical pulse of SBSL (dotted line) is shown. Then, the next graph shows the central part temperature of the bubble increasing from ~ 3000 K to $\sim 17\,000$ K. We notice that the central part temperature of the d case is $\sim 21,000$ K when the chemical reaction is ignored in the calculation, a decrease of about 4000 K due to the chemical dissociation. The result is not shown here. The following graphs show that the central part number density of water vapor decreases as the temperature increases and that when the temperature exceeds 10 000 K (c and d case) most of the water vapor is dissociated to O and H atoms, and some small part of O_2, H_2, and OH molecules. The perceptible flash is within the duration (-0.2 ns, 0.2 ns), see the first graph, therefore, the contribution from
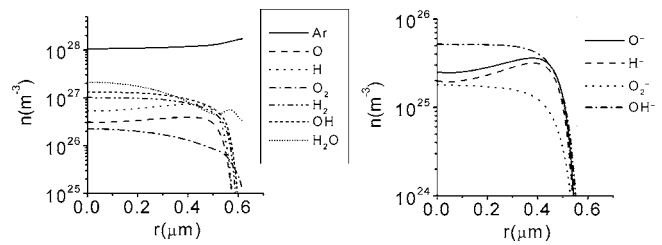

FIG. 3. Distribution of the gas contents and the negative ions inside an Ar bubble at its minimum size in 20 °C water. Other parameters see Table I.

RAEA would be much larger than that from RAEM in this case, which results in the second graph (from the left) in Fig. 1. The situation is similar to the case of a He or Xe bubble in 0 °C water. However, the ionization potential of Xe is the lowest, of Ar higher, and of He the highest, therefore, the ionized electron number in the Xe bubble would be the largest, in the Ar bubble smaller, and in the He bubble smallest. Accordingly, concerning the EAB+EIBR part, the emitted photon number of the Xe bubble is the largest, of the Ar bubble is smaller, and of the He bubble is the smallest. That is the case shown in the first three graphs (from the left) in Fig. 1. We noticed that the other calculation [21] shows the contribution from RAEA, compare to the contribution from EAB+EIBR, is of comparable importance for SBSL of the Ar and He bubble at room temperature water, but it is insignificant in 0 °C water. The reason may be that, as we mentioned in the Introduction, in [21] (and also in [20]) too small amount of water vapor is retained in the collapsing bubble which follows that too small amount of O and H atoms is produced, and naturally the contribution from RAEA is minor.

In other cases when the maximum temperature in the bubble may not be high enough to dissociate most of the molecules into atoms, the situation changes. For example, in the case of an Ar bubble in 20 °C water (parameters see Table I), the distributions of the gas contents and the various negative ions in the bubble at its minimum size are illustrated in Fig. 3. Apparently, except the Ar atoms, there are mostly H_2O, OH, H_2 molecules at the center part of the bubble (the left graph), and among the negative ions, OH^- is most. The situation is similar to the case of an Ar bubble in 34 °C water. That may help to understand why the RAEM contributes the most for SBSL as one can see from the last two graphs (from the right) in Fig. 1.

Validity of the assumption of the chemical equilibrium in the present model

The validity of the application of the law of mass action to the present model can be verified by the comparison of the so-called time scales [14]: the dynamic time scale of the bubble motion t_{dyn}, the mass diffusion time scale t_{dif}, the chemical reaction time scale t_{chm}, and the ionization time scale t_{ion}. As a typical example, we consider the process of Eq. (3) in calculating t_{chm} Then

$$t_{dyn} = \frac{R}{\dot{R}}, \tag{17}$$

TABLE II. Time scales of the bubble motion and the chemical dissociation at the points b, c, and d in Fig. 2.

	b	c	d
t_{dyn}	6.2×10^{-10} s	5.1×10^{-10} s	5.0×10^{-10} s
t_{chm}	3.5×10^{-10} s	4.4×10^{-11} s	2.2×10^{-11} s

$$t_{chm} = R\sqrt{\rho_1(0)K_p(\mathrm{H_2O})}, \tag{18}$$

$$t_{\mathrm{ion}} = \min[R\sqrt{\rho_2(0)K_{p2}(e)}, R\sqrt{\rho_1(0)K_{p1}(e)}], \tag{19}$$

where $K_p(\mathrm{H_2O})$ is the dissociative equilibrium constants of the chemical reaction (3), $K_{p1}(e)$, $K_{p2}(e)$ are the ionization equilibrium constants of the Saha equation for water vapor and Ar atom, respectively, and $\rho_1(0)$, $\rho_2(0)$ are the vapor and Ar density at the center of the bubble, respectively. The expression of t_{dif} can be found in [14] which shows $t_{\mathrm{dif}} \gg t_{\mathrm{dyn}}$ when the bubble is at its collapsing phase. It means that it is reasonable to ignore the diffusion of those chemical products of water vapor, because as shown in Fig. 2, the chemical reactions mainly take place as the bubble at its collapsing phase. For the same reason, we evaluate the time scales t_{dyn} and t_{chm} at points b, c, and d in Fig. 2 and list them in Table II. Here we see $t_{\mathrm{dyn}}(b) > t_{\mathrm{chm}}(b)$, and $t_{\mathrm{dyn}} \gg t_{\mathrm{chm}}$ for c and d points. The results mean that at least at the bubble collapsing phase the assumption of the chemical equilibrium is a good approximation. In addition, the ionization mainly takes place as the bubble is at its flashing phase, see the first graph in Fig. 2. We calculate the time scales when the bubble is at its "hottest" phase, $t_{\mathrm{ion}} = 1.2 \times 10^{-9}$ s, which is much smaller than $t_{\mathrm{dyn}} = 1.4 \times 10^{-8}$ s at that moment. It shows that the Saha equation inside a sonoluminescing bubble getting to its hottest phase is a good approximation too, since the evaluation of the ionization is important only at the vicinity of this moment.

Spectrum of SBSL and blackbody radiation

An often mentioned important character of SBSL is the blackbody radiationlike spectrum [8,9]. The numerical simulation shows that the maximum temperature inside a sonoluminescing bubble is about 10 000 K–30 000 K. The bremsstrahlung and recombination model (EAB+EIBR) alone, in such a temperature, cannot produce the blackbody radiation type spectrum. Hammer and Frommhold try to reproduce the SBSL spectrum by EAB+EIBR [33], but we see the devia-
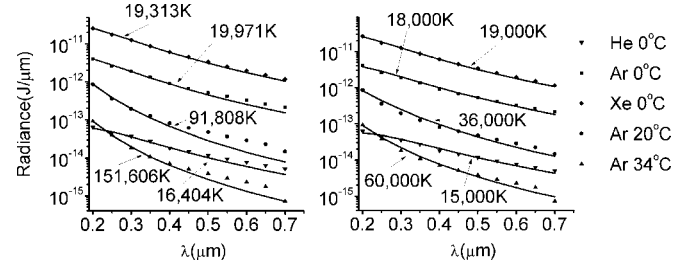

FIG. 5. Spectra of SBSL from different gas bubbles (filled squares), and their best (left), or looking best (right), fit to the blackbody radiation formula (solid lines), the data are the same as those in Fig. 4 but they are with logarithm scale. The numbers with arrows are the temperatures fitted by the blackbody radiation formula.

tion between the calculated spectrum and the blackbody radiationlike experimentally measured one is considerable (compared to the consistency appearing in Fig. 4), moreover, referring to the experimental data of the spectrum quoted in the Fig. 13 of Ref. [33], the transmission corrections [7] should have been considered. With our model, namely EAB+EIBR+RAEA+RAEM, the calculated spectrum can be well fitted by the blackbody radiation formula. Figure 4 demonstrates the spectra from different gas bubbles. They look like the perfect blackbody radiation, but if we illustrate them in the logarithm scale, we will see some deviations, see the left graph of Fig. 5. We may adjust the temperature of the blackbody radiation formula and make the fit in logarithm scale "look best" as shown in the right graph of Fig. 5. There are some differences between the temperatures best fitted or "looking best fitted" in the case of He, Ar, or Xe in 0 °C water, which grow even more distinct in the case of Ar in 20 °C or 34 °C water. The reason is that the wavelength range in SBSL is only 0.2–0.7 μm, it is narrow, therefore, the fit cannot be accurate, for example, an observed spectrum is fitted by the blackbody radiation formula, the fitted temperature was 25 000 K [8] and the fit looks very good, but in Ref. [11] the best fitted temperature is suggested as 40 000 K. Moreover, in Fig. 4 we may see the Ar bubble in different ambient temperatures, the brighter bubble corresponds to the lower fitted blackbody radiation temperature. Similar trend one may find in Figs. 5–9 of Ref. [9] and the results illustrated in Fig. 11 of Ref. [33]. In this sense, we may believe that the temperature fit to the blackbody radiation formula is meaningless. To further deepen this idea, we demonstrate the temperature distribution as the bubble getting the hottest in Fig. 6. Comparing the temperatures in
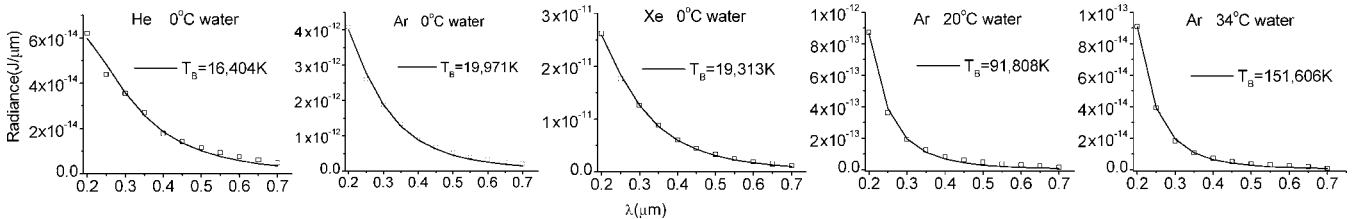

FIG. 4. Spectra of SBSL from different gas bubbles (hollow squares) and their best fit to the blackbody radiation formula (solid lines), where T_B is the temperature fitted by the blackbody radiation formula.
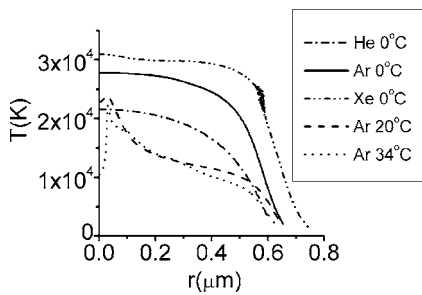
FIG. 6. Calculated distributions of temperature of the different gas bubbles as the bubble getting the hottest. For the other corresponding parameters see Table I.

Figs. 5 and 6 we may find that there are no reasonable connections between them. To further understand this phenomena, the research of the coefficient of absorption of the SBSL bubbles may be interesting.

It must be mentioned that the spectrum of SBSL Xe bubble has a maximum at $\lambda \sim 0.3$ μm [7], this typical shape of the spectrum was first understood by Moss *et al.* [34]. This phenomenon cannot be interpreted in the present model, but results in Fig. 6 may provide a hint. Figure 6 shows that the Xe bubble reaches highest maximum temperature $\sim 31\,000$ K, which is advantageous to the excitation of OH radicals, thus the broadened line spectrum of the process $OH^* \rightarrow OH + h\nu$ may affect the shape of the spectrum.

Distribution of the coefficient of absorption

The coefficient of absorption κ_λ of the different radiation mechanisms may provide more precise information of the SBSL. Different temperature results in different distribution of ionized electrons and the κ_λ. Again in the case of an Ar bubble in 0 °C water (the other parameters are the same as in Table I), the distributions of the temperature and the number densities of electrons (with logarithm scale) inside the
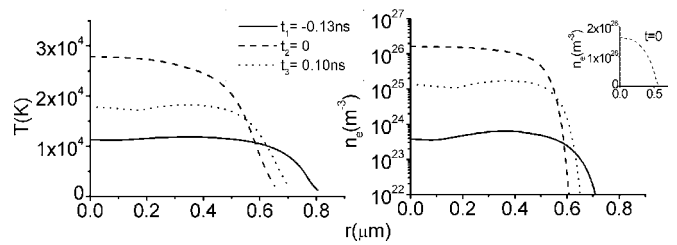

FIG. 7. Spatial profiles of the calculated temperatures (left) and number densities of electrons (right) inside an Ar bubble in 0 °C water (same as in the case in Fig. 2) for the bubble at the vicinity of its minimum size.

bubble at the vicinity of its minimum size are illustrated in Fig. 7. The number density of electron at $t=0$ reaches as high as $\sim 10^{26}/m^3$, when the temperature is about 28 000 K. The maximum temperature ($\sim 28\,000$ K) actually is ~ 8000 K lower than that when the chemical dissociation absents in the calculation. From Fig. 7 we see when the temperature decreases, the number density of electron decreases fast, therefore, the duration of SBSL is short. The inset to the right graph in Fig. 7 is the distribution of the number density of electron at $t=0$, but with linear scale, we can clearly see that the high density of electron is mainly in the center part of the bubble. That may interpret why people tend to believe that the flash of SBSL comes out of the center part of the bubble [35]. Corresponding to the case in Fig. 7, the product of the coefficient of absorption κ_λ and the radius R instead of κ_λ are illustrated in Fig. 8, thus we may easily perceive that if $\kappa_\lambda R \ll 1$ it means the bubble is optically thin body and if $\kappa_\lambda R \gg 1$ it is optically thick. In Fig. 8, $t=-0.13$ ns, corresponding to $T \sim 10\,000$ K at center part, and $t=0.10$ ns, $T \sim 18\,000$ K, the bubble is optically thin body and the RAEA dominates the radiation; $t=0$, $T \sim 28\,000$ K, the RAEA still dominates the radiation for $\lambda=200$ nm and $\lambda=400$ nm, but does not for $\lambda=700$ nm, when the contribution from the EAB exceeds that from the RAEA. Therefore, we may con-
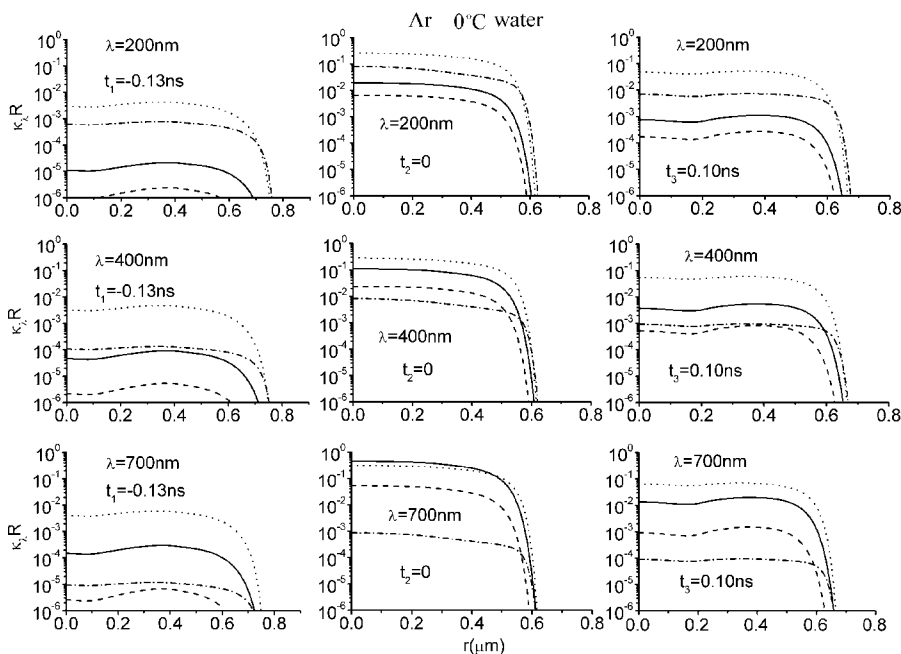

FIG. 8. Product of the absorption coefficient (κ_λ) and the bubble radius (R) for wavelength 200 nm, 400 nm, and 700 nm, corresponding to the cases in Fig. 7. Where the solid lines denote the electron-neutral atom bremsstrahlung (EAB), the dashed lines the electron-ion bremsstrahlung and recombination (EIBR), the dotted lines the radiative attachment of electrons to oxygen and hydrogen atoms (RAEA) and the dash-dotted lines the radiative attachment of electrons to oxygen molecules and OH radicals (RAEM), respectively.
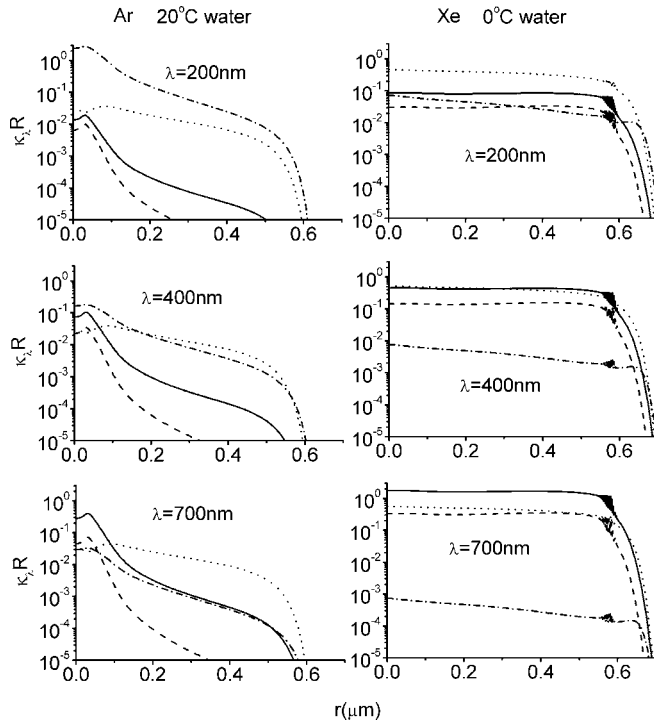
FIG. 9. Product of the absorption coefficient (κ_λ) and the bubble radius (R) for wavelength 200 nm, 400 nm, and 700 nm, for the cases of an Ar bubble (left column) in 20 °C and a Xe bubble (right column) in 0 °C water (the other parameters see Table I) getting to their hottest phase. Here the solid lines denote the electron-neutral atom bremsstrahlung (EAB), the dashed lines the electron-ion bremsstrahlung and recombination (EIBR), the dotted lines the radiative attachment of electrons to oxygen and hydrogen atoms (RAEA) and the dash-dotted lines the radiative attachment of electrons to oxygen molecules and OH radicals (RAEM), respectively.

clude that, in general, the higher the temperature is, the larger the contribution from the EAB is. As the temperature increases, the contribution of the EAB and EIBR gradually emerges.

In other cases, the situation may be different. As we see in Fig. 6, the temperatures of different bubbles at the hottest-phase are very different. So are the gas contents resulting from the chemical reaction (compare Figs. 2 and 3), which would cause the different κ_λ in the bubbles. In Fig. 9, for the cases of an Ar bubble in 20 °C and a Xe bubble in 0 °C water, we demonstrate the spatial profiles of $\kappa_\lambda R$ when the bubble is at its hottestphase. For the Ar bubble in 20 °C water, at the moment (for the temperature, refer to Fig. 6), the RAEM dominates the radiation for $\lambda = 200$ nm. It is similar to the RAEA for $\lambda = 400$ nm, and the RAEA dominates the radiation for $\lambda = 700$ nm. For the Xe bubble in 0 °C water, at the moment, the corresponding temperature of $T \sim 30\,000$ K (see Fig. 6), the RAEA dominates the radiation for $\lambda = 200$ nm. It is similar to the EAB for $\lambda = 400$ nm, and the EAB dominates the radiation for 700 nm. In the situation of SBSL in water, RAEM or RAEA contributes most to ultraviolet (UV) part, which results in UV part in the SBSL spectrum is raised. The higher is UV part in spectrum, the higher is the temperature fitted by the blackbody radiation formula. That is why those SBSL bubbles under higher am-
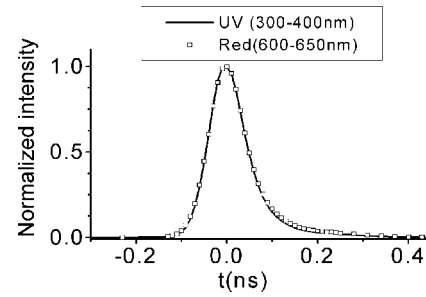

FIG. 10. Comparison of the calculated normalized optical pulses of UV and red from an Ar bubble in 0 °C water, corresponding to the case in Fig. 2.

bient temperature correspond to the higher blackbody radiation temperature, though these bubbles may be darker. Since higher ambient temperature means higher vapor pressure, there is more residual water vapor and so are the dissociated products retaining inside these bubbles as the bubbles are at their flashing phase, therefore, in these bubbles RAEA or RAEM dominates SBSL. On the other hand, from Figs. 8 and 9 we can see that the bubbles are neither optically thick body nor ideal optically thin body. It may help prove that the blackbody radiationlike spectrum of SBSL means nothing. Instead, it may be just a coincident.

Optical pulses of SBSL

Concerned with the mechanism of SBSL, the FWHM of the optical pulse is usually an important quantity. In fact, the simple bremsstrahlung and recombination model [12] is built upon the evidence that it can well interpret the experimentally observed FWHM, though the water vapor effects are absent. In the present model, though the radiative attachment of electrons to oxygen and hydrogen atoms (RAEA) and to oxygen molecules and OH radicals (RAEM) dominates the SBSL (the electron-neutral atom bremsstrahlung may be important in the Xe bubble, too, see the middle graph in Fig. 1), the calculated normalized optical pulses of red and UV still almost overlap for Ar bubble in 0 °C water, as demonstrated in Fig. 10. It is consistent with the observation [5]. We present more data of the FWHM of the various different gas bubbles in different ambient temperatures. Figure 11 demonstrates these FWHM's of Ar, Xe, and He bubbles vs 50 nm interval of wavelength. We notice that there is an apparent
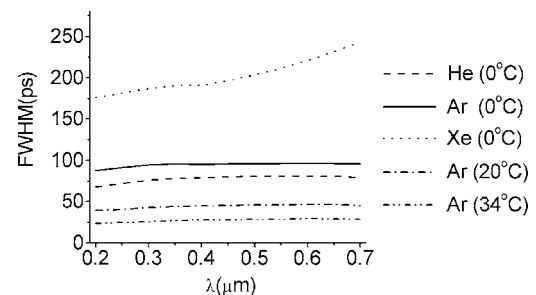

FIG. 11. Wavelength dependence of FWHM's of bubbles filled with He, Ar, and Xe, in 0 °C, 20 °C, and 34 °C water, respectively. The other parameters are the same as in Table I.
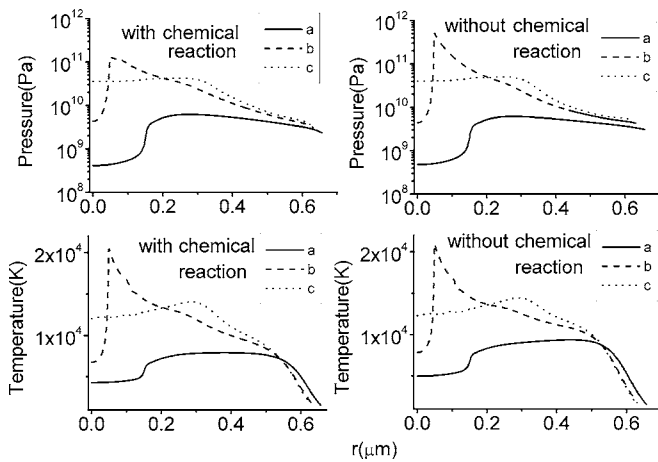
FIG. 12. Spatial profiles and time distribution of the calculated pressure and temperature in an Ar bubble grown in water at 34 °C, the corresponding parameters are given in Table I. The left graphs represent the results of the chemical reaction being considered, while the right graphs represent the results of the chemical reaction being ignored. Here *a*, *b*, and *c* denotes the time sequence of t_a = −0.036 ns, t_b = −0.020 ns, and t_c = −0.015 ns, respectively. $t=0$ is set when the bubble is at its minimum size.

FIG. 13. Spatial profiles and time distribution of the calculated number densities of various particles, H_2O, OH, O_2, H_2, O, and H, corresponding to the case in Fig. 12, and *a*, *b*, and *c* denotes the same time sequence as that in Fig. 12.

dependence of wavelength for the FWHM's of the Xe bubble, and just a slight dependence of wavelength for the FWHM's of the other bubbles, including Ar bubble in 0 °C water, of which the normalized optical pulses of red and UV overlap (see Fig. 10).

Shock wave and chemical dissociation

In the last graph of Fig. 1, one may see a convex kink in the curve of the optical pulse of the Ar bubble in 34 °C water which results from the shock formation inside the bubble, as argued in [22]. Probably it is a clue to measure the shock formation inside the bubble. If the first order correction to Mach number is considered in the RP equation, such as the Keller-Miksis formulation [36], then the shock formation disappears [22]. Xu *et al.* [37] employed the modified Keller formulation of RP equation in their calculation and with which they caught the shock formation in SBSL Xe bubble, but not in Ar bubble. Someone would argue that the modified RP equation with the first order correction to Mach number should be considered, since the correction embodies the compressibility of the liquid. There would be difficulty, in fact, the first order correction to the Mach number is only valid in the case $M \ll 1$, referring to SBSL bubble, this condition never matches as the bubble is at its collapsing phase. While the compressibility of the liquid may have the considerable effect on the bubble motion only when the bubble is in a collapsing phase, other cases the effect is negligible. Therefore, in the case of SBSL calculation, that whether the first order correction to the Mach number in the RP equation can effectively cover the effect of the compressibility of the liquid to the bubble motion is skeptical.

Back to the case of the argon bubble in 34 °C water, the numerical calculation demonstrates the shock formation inside the bubble. In fact, the preponderance of water vapor
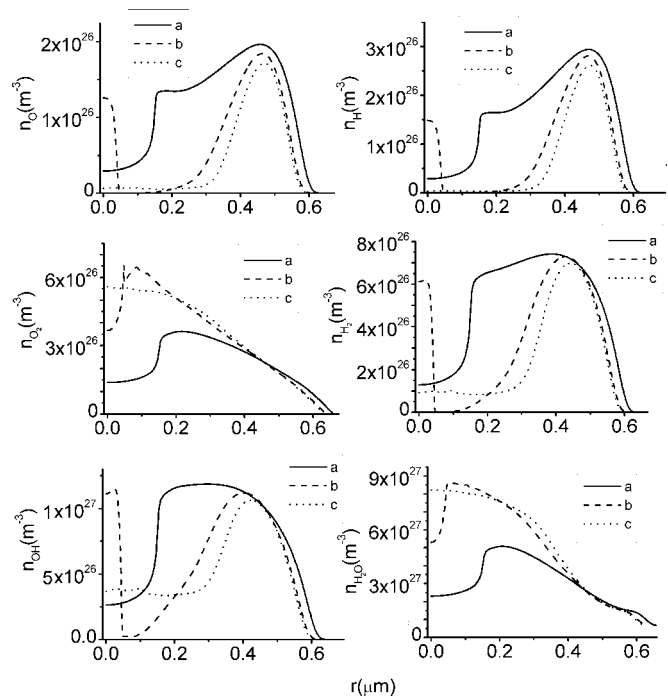
degrades the increase of the temperature in the bubble, but promotes the excitation of shock wave [34]. The left graphs of Fig. 12 shows the results with considering the chemical reactions. It can be seen that the shock wave develops near the center of the bubble, and it converges at the bubble center and creates a very high pressure and temperature. We may find that the maximum speed of this convergent shock wave reaches ~10 000 m/s at the vicinity of the bubble center. The wave heats the center of the bubble to a high temperature of ~2.0×10^4 K within a very short duration of ~5 $\times 10^{-14}$ s which is too short to contribute a large amount of the photon. Comparing the case when the chemical reactions are ignored in the calculation (the right graphs), the chemical reaction has a very slight affection on the shock formation. The reason lies in the existence of the excluded volume [38]. In the formulas of chemical dissociation, there are factors $\exp[-(\tilde{\nu} - \nu_e)b_{H_2}/(1 - \Sigma_i \nu_i b_i)]$ and $\exp[-(\tilde{\nu} - \nu_e)b_{H_2O}/(1 - \Sigma_i \nu_i b_i)]$, see Appendix A, which are caused by van der Waals hard core, the excluded volume. These factors suppress the chemical dissociation when the local pressure gets very high, such as at the region where the shock wave develops. In Fig. 13, we may clearly perceive it. At the shock wave front though the temperature is very high, the pressure is also extremely high which suppresses the chemical dissociation that should have taken place. That is why at shock wave front there are almost no oxygen or hydrogen atoms and thus few chemical dissociation, and the shock formation is almost not weakened. To avoid the divergence in the calculation, we technically limit the hard core $\Sigma_i \nu_i b_i \leqslant 0.96$, which we believe is large enough.
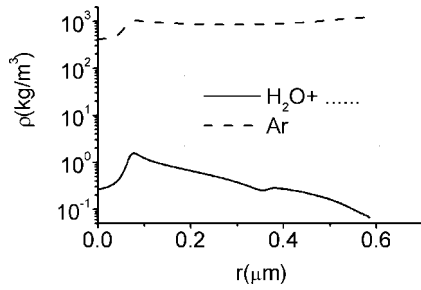
FIG. 14. Densities of the argon gas and the vapor + its chemical products when the bubble is at its minimum size, for an Ar bubble in 20 °C 85 wt. % H_2SO_4, $R_0 = 4.55$ μm, $f = 30$ KHz, and $P_a = 2.3$ bar.

SBSL in low vapor pressure liquids

SBSL may be observed from a low vapor pressure liquids [3,39,40], when there is only little vapor of surrounding liquid evaporating into the bubble and the vapor effects are minor. We may expect the temperature in this kind of bubble to get very high and then a hot plasma core may form in the bubble [3]. That is why the line spectrum of Ar atoms appears. In the present work, we apply our model to the case of an Ar bubble in 20 °C 85 wt. % H_2SO_4, and driving frequency 30 kHz and driving acoustic pressure 2.3 bar. Because the ambient radius R_0, the maximum radius of the bubble R_M and acoustic frequency are not provided in Ref. [3], we cannot obtain the adjusted driving acoustic pressure [22] and have to simply take the measured one 2.3 bar and set $R_0 = 4.55$ μm, therefore, the calculation is a kind of "concept calculation" cannot directly compare with the experimental data. When the temperature is below 400 K, the water vapor pressure of 85 wt. % H_2SO_4 is much higher than H_2SO_4 vapor pressure; when the temperature at the bubble wall exceeds 400 K, the bubble will be in the collapsing phase and the duration will be too short to consider the mass exchange by the evaporation and condensation of vapor. Therefore, as a good approximation only the water vapor is considered in the calculation. Figure 14 shows that there is only little water vapor and its chemical products retaining in the bubble when the bubble is at its minimum size. Figure 15 shows the pressure and the temperature inside the bubble. We may see a weak shock formation at the center of the bubble and the temperature as high as ~120 000 K when the chemical reaction and the ionization are considered. The high temperature is enough to stimulate the radiation of the line spectrum of Ar atom, which is consistent with the observation [3]. As shown in Fig. 14, there is too little vapor inside the bubble and the associated chemical reactions have little affection, therefore, the ionization mainly affect the temperature, which decreases the maximum temperature of ~130 000 K (compare the two lower graphs in Fig. 15).

We may evaluate the coefficient of absorption in such a high temperature bubble. Figure 16 shows that the contribution from the EAB and EIBR dominates the SBSL, while the RAEA and the RAEM have little contribution. For the relatively long wavelength part the bubble is optically thick body, while for UV (200 nm) it is neither thick nor thin. It is natural that the spectrum can be well fitted by the blackbody
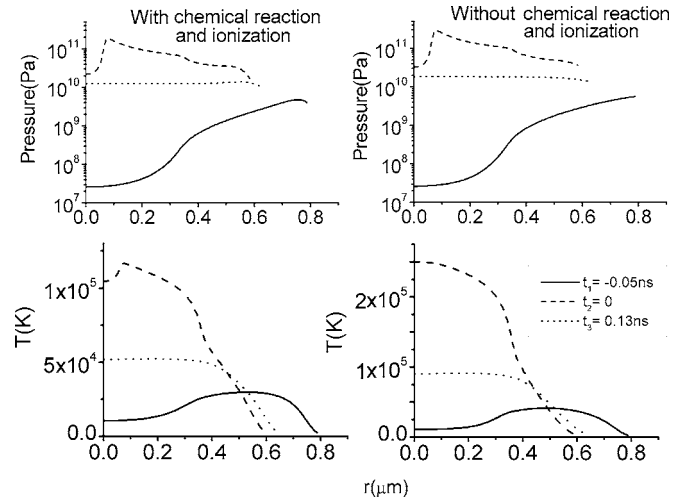

FIG. 15. Spatial profiles and time distribution of the calculated pressure and temperature, the corresponding parameters are the same as in Fig. 14. The left graphs represent the results with the chemical reaction and ionization being considered, while the results with the chemical reaction and ionization being ignored are illustrated in the right graphs. $t = 0$ is set when the bubble is at its minimum size.

radiation formula, see Fig. 17. However, what is unusual is that the fitted temperature is only ~30 000 K, much lower than ~120 000 K, the maximum temperature calculated from the gas dynamics model, see Fig. 15. This again verifies the argument that the blackbody radiation like spectrum of SBSL means nothing. It is just a coincident.

CONCLUSION

The partial differential equations of fluid mechanics in conjunction with the earlier form of RP equation and the energy balance equation in the surrounding liquid are numerically solved. The temperature and pressure, the gas contents dissociated from water vapor and ionized electrons, the coefficient of absorption, and the emitted photon numbers of SBSL from the different radiation mechanisms are calculated. The time-scales argument is clarified upon the validity of the application of the mass action law to the present model. When the bubble approaches the collapsing phase, the assumption of the chemical equilibrium is reasonable, and at the bubble flashing phase the Saha equation would be a good approximation, too. For the cases of an Ar bubble in 20 °C or 34 °C water, the temperature cannot get very high and there are plenty of molecules, such as O_2 and OH radicals, retaining in the bubble. In these cases the radiative attachment of electrons to O_2 and OH dominates the SBSL; for the other cases, such as an Ar or a He bubble in 0 °C water, the temperature is high enough to dissociate most of the water vapor into oxygen and hydrogen atoms, therefore, the radiative attachment of electrons to oxygen and hydrogen atoms dominates the SBSL; for the case of a Xe bubble in 0 °C water, the temperature get so high that the contribution from the electron-neutral atom and the electron-ion bremsstrahlung and recombination is as large as that from the ra-
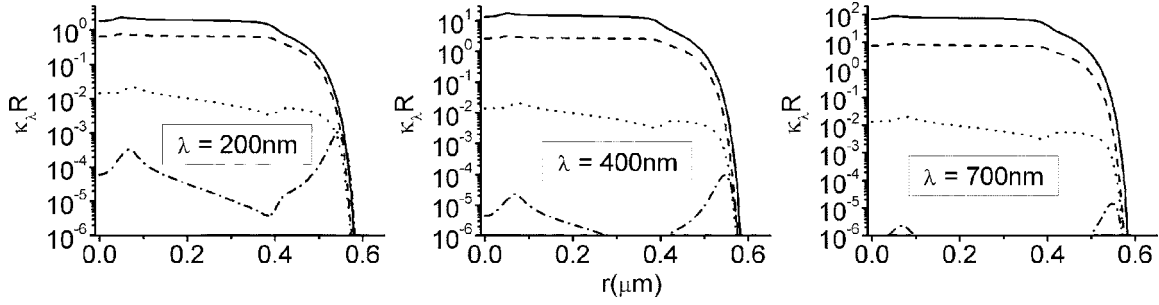
FIG. 16. Product of the absorption coefficient (κ_λ) and the bubble radius (R) for wavelength 200 nm, 400 nm, and 700 nm, for the case in Fig. 14. Here the solid lines denote the electron-neutral atom bremsstrahlung (EAB), the dashed lines the electron-ion bremsstrahlung and recombination (EIBR), the dotted lines the radiative attachment of electrons to oxygen and hydrogen atoms (RAEA) and the dash-dotted lines the radiative attachment of electrons to oxygen molecules and OH radicals (RAEM), respectively.

diative attachment of electrons to oxygen and hydrogen atoms, and they together dominate the SBSL. With the present model, we also provide good interpretations to the experimental results, such as the FWHM of the optical pulse and the spectrum of SBSL. We find that it is only a coincidence that the spectrum of SBSL has the blackbody radiation feature, and that the fitted blackbody radiation temperature actually has no connection to the temperature inside the bubble. For the case of an Ar bubble in 34 °C water, we find that the chemical dissociation has little affection on the shock formation, because the high pressure at the shock wave front results in the large excluded volume at that local and the chemical dissociation being suppressed there.

For the case of the SBSL in the liquid with low vapor pressure, the temperature inside the bubble can get very high. In this case the bubble may be almost an optically thick body, and the electron-neutral atom bremsstrahlung, the electron-ion bremsstrahlung and recombination dominates the SBSL. In this case, we find the fitted blackbody radiation temperature still has no connection to the real temperature inside the bubble.

We try to interpret all the experimental observation with the present model quantitatively or qualitatively, however, there is an important experimental phenomenon cannot be included in the discussion, it is the spectrum of SBSL of Xe bubble. The spectrum has the maximum at $\lambda \sim 0.3$ μm [7] and it seems to arise from the broadened OH line. However, somebody would believe that the peak at $\lambda \sim 0.3$ μm results from the mechanism of the bremsstrahlung and recombina-

tion [11], therefore, the contribution from the radiative attachment should be absent or negligible, otherwise this peak might vanish. If it is true, neither can we answer what dynamical mechanism empties the whole vapor from the Xe bubble when the bubble collapses, nor can answer what makes the Xe bubble so different from the Ar bubble in which the vapor effect is such an obvious phenomenon as observed in the experiment [13]. This is still an open question.

APPENDIX A

By the law of mass action, the dissociative equilibrium constants of the reaction (3)–(6) are as follows, respectively:

$$K_p(\mathrm{H_2O}) = \frac{g_{\mathrm{H_2O}}}{g_{\mathrm{OH}}g_{\mathrm{H}}} \frac{K_0(\mathrm{H_2O})}{T^2} \frac{1 - \exp\left(-\dfrac{\hbar\omega_{\mathrm{OH}}}{kT}\right)}{\sum\limits_i^3 \left[1 - \exp\left(-\dfrac{\hbar\omega_i}{kT}\right)\right]}$$

$$\times \exp\left[\frac{(\tilde{\nu} - \nu_e)b_{\mathrm{H_2}}}{1 - \sum\limits_i \nu_i b_i} + \frac{\varepsilon_{\mathrm{H_2O}}}{kT}\right],$$

$$K_0(\mathrm{H_2O}) = 2\pi^2\hbar^2 \frac{(I_1 I_2 I_3)^{1/2}}{I_{\mathrm{OH}}k^2} \left(\frac{m_{\mathrm{H_2O}}}{m_{\mathrm{OH}}m_{\mathrm{H}}}\right)^{3/2}$$

$$= 9.64 \times 10^{-5} \ (\mathrm{Pa^{-1}}), \qquad (\mathrm{A1})$$

$$K_p(\mathrm{OH}) = \frac{g_{\mathrm{OH}}}{g_o g_{\mathrm{H}}} \frac{K_0(\mathrm{OH})}{T^{3/2}} \frac{1}{1 - \exp\left(-\dfrac{\hbar\omega_{\mathrm{OH}}}{kT}\right)}$$

$$\times \exp\left[\frac{(\tilde{\nu} - \nu_e)b_{\mathrm{H_2}}}{1 - \sum\limits_i \nu_i b_i} + \frac{\varepsilon_{\mathrm{OH}}}{kT}\right],$$
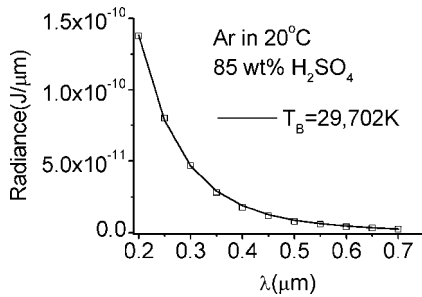

FIG. 17. Spectrum of SBSL (filled squares) and its best fit to the blackbody radiation formula (solid lines), for the case in Fig. 14, where T_B is the temperature fitted by the blackbody radiation formula.

$$K_0(\text{OH}) = 2\hbar I_{\text{OH}} \left(\frac{2\pi m_{\text{OH}}}{m_{\text{O}} m_{\text{H}} k} \right)^{3/2} = 1.51 \times 10^{-5} \ (\text{Pa}^{-1}),$$

(A2)

$$K_p(\text{O}_2) = \frac{g_{\text{O}_2}}{g_{\text{O}}^2} \frac{K_0(\text{O}_2)}{T^{3/2}} \frac{1}{1 - \exp\left(-\dfrac{\hbar\omega_{\text{O}_2}}{kT} \right)}$$

$$\times \exp\left[\frac{(\tilde{\nu} - \nu_e) b_{\text{H}_2\text{O}}}{1 - \sum_i \nu_i b_i} + \frac{\varepsilon_{\text{O}_2}}{kT} \right],$$

$$K_0(\text{O}_2) = \hbar I_{\text{O}_2} \left(\frac{4\pi}{m_{\text{O}} k} \right)^{3/2} = 4.06 \times 10^{-6} \ (\text{Pa}^{-1}), \quad \text{(A3)}$$

$$K_p(\text{H}_2) = \frac{g_{\text{H}_2}}{g_{\text{H}}^2} \frac{K_0(\text{H}_2)}{T^{3/2}} \frac{1}{1 - \exp\left(-\dfrac{\hbar\omega_{\text{H}_2}}{kT} \right)}$$

$$\times \exp\left[\frac{(\tilde{\nu} - \nu_e) b_{\text{H}_2}}{1 - \sum_i \nu_i b_i} + \frac{\varepsilon_{\text{H}_2}}{kT} \right],$$

$$K_0(\text{H}_2) = \hbar I_{\text{H}_2} \left(\frac{4\pi}{m_{\text{H}} k} \right)^{3/2} = 6.39 \times 10^{-6} \ (\text{Pa}^{-1}), \quad \text{(A4)}$$

where g_i is the statistical weight of the ground state and m_i is the mass for ($i = \text{H}_2\text{O}, \text{OH}, \text{O}_2, \text{H}_2, \text{O}, \text{H}$), I_i, ω_i, for ($i = 1, 2, 3$), I_k, ω_k ($k = \text{OH}, \text{O}_2, \text{H}_2$) are the principal moment of inertia and vibrational angular frequencies of water vapor and of OH radical, O_2, H_2, respectively. Then, approximately, the number density of dissociated particles can be evaluated as

$$\frac{n_{\text{H}_2\text{O}}}{n_{\text{OH}} n_{\text{H}}} = \frac{P}{N} K_p(\text{H}_2\text{O}), \quad \text{(A5)}$$

$$\frac{n_{\text{OH}}}{n_{\text{O}} n_{\text{H}}} = \frac{P}{N} K_p(\text{OH}), \quad \text{(A6)}$$

$$\frac{n_{\text{O}_2}}{n_{\text{O}}^2} = \frac{P}{N} K_p(\text{O}_2), \quad \text{(A7)}$$

$$\frac{n_{\text{H}_2}}{n_{\text{H}}^2} = \frac{P}{N} K_p(\text{H}_2), \quad \text{(A8)}$$

where n_i is the number density for ($i = \text{H}_2\text{O}, \text{OH}, \text{O}_2, \text{H}_2, \text{O}, \text{H}$), P the pressure, and N the number density of the total particles.

With the Saha equation, the number densities of positive ions can be evaluated from

$$\frac{n_i}{n_i^+ n_e} = \frac{P}{N} K_{pi}(e), \quad \text{(A9)}$$

TABLE III. The statistical weight g of some atoms, molecules and ions.

	He	Ar	Xe	H$_2$O	OH	O$_2$	H$_2$	O	H
Atom or molecule	1	1	1	1	4	3	1	9	2
Positive ion	2	6	6	4	3	4	2	4	1
Negative ion					1	4		6	1

$$K_{pi}(e) = \frac{g_i}{2 g_i^+} \left(\frac{h^2}{2\pi m_e} \right)^{3/2} \frac{1}{(kT)^{5/2}} \exp[(I_i^+ - \Delta I_i)/kT],$$

(A10)

where n_i denotes the number density of all the atoms and molecules, m_e is the mass of electron, k the Boltzmann constant, g_i and g_i^+ the statistical weight of the ground state before and after ionization, respectively; I_i^+ the ionization potential, and ΔI_i the reduction of the ionization potential of the ith molecule or atom, respectively. The ΔI_i takes the same value as that in [21]. For those negative ions

$$\frac{n_j^-}{n_j n_e} = \frac{P}{N} K_{pj}(a), \quad \text{(A11)}$$

$$K_{pj}(a) = \frac{g_{j^-}}{2 g_j} \left(\frac{h^2}{2\pi m_e} \right)^{3/2} \frac{1}{(kT)^{5/2}} \exp[I_j/kT], \quad \text{(A12)}$$

where n_j denotes the number density of OH O$_2$, O, H, and g_i^- is the statistical weight of the negative ion, the electron affinity $I_{\text{O}_2}^- = 0.46$ eV, $I_{\text{OH}}^- = 1.83$ eV, $I_{\text{O}}^- = 1.465$ eV, $I_{\text{H}}^- = 0.754$ eV. We have noticed that the statistical weight g affects the numerical results, and list them in Table III for convenience. With the formulas (A1)–(A12), we may evaluate the number density of all the particles.

APPENDIX B

The extrapolating formulas of the free-free atomic absorption coefficient for electron-neutral atom bremsstrahlung per unit electron density (in cm^5) for $T > 20\,000$ K are

$$\sigma_{\text{He}(\lambda = 0.5 \ \mu\text{m})} = 2.02488 \times 10^{-40} + 2.37992 \times 10^{-44} T,$$

$$\sigma_{\text{He}(\lambda = 1.0 \ \mu\text{m})} = 4.6 \times 10^{-40} + (1.59 \times 10^{-43} + 8.7619$$
$$\times 10^{-49} T) T, \quad \text{(B1)}$$

$$\sigma_{\text{Ar}(\lambda = 0.5 \ \mu\text{m})} = 0.15764 \times 10^{-40} + (2.60974 \times 10^{-44}$$
$$+ 1.28106 \times 10^{-48} T) T,$$

$$\sigma_{\text{Ar}(\lambda = 1.0 \ \mu\text{m})} = 0.18474 \times 10^{-40} + (3.95124 \times 10^{-44}$$
$$+ 1.13766 \times 10^{-47} T) T, \quad \text{(B2)}$$

$$\sigma_{\text{Xe}(\lambda = 0.5 \ \mu\text{m})} = 0.31415 \times 10^{-40} + 1.41 \times 10^{-43} T,$$

$$\sigma_{\text{Xe}(\lambda = 1.0 \ \mu\text{m})} = -41.61667 \times 10^{-40} + 8.77 \times 10^{-43} T,$$

(B3)

$$\sigma_{O(\lambda=0.5\ \mu m)} = 0.42354 \times 10^{-40} + 2.76987 \times 10^{-44}T,$$

$$\sigma_{O(\lambda=1.0\ \mu m)} = 0.41474 \times 10^{-40} + (9.38705 \times 10^{-44}$$
$$+ 3.00712 \times 10^{-48}T)T, \quad \text{(B4)}$$

$$\sigma_{H(\lambda=0.5\ \mu m)} = 10.61429 \times 10^{-40} + (1.87075 \times 10^{-45}$$
$$+ 6.07386 \times 10^{-49}T)T,$$

$$\sigma_{H(\lambda=1.0\ \mu m)} = 30.56667 \times 10^{-40} + 2.26 \times 10^{-43}T. \quad \text{(B5)}$$

Besides, we find a good interpolating formula for those wavelength $\lambda < 1.0\ \mu m$, which is

$$\sigma_{\lambda} = \sigma_{\lambda=1.0\ \mu m}\lambda^{(\ln \sigma_{\lambda=1.0\ \mu m}/\sigma_{\lambda=0.5\ \mu m})/\ln 2}, \quad \text{(B6)}$$

where λ is in μm. Then the absorption coefficient can be evaluated as

$$\kappa_{\lambda,e-a} = \sigma_{\lambda,i}n_i n_e, \quad \text{(B7)}$$

where i denotes those atoms above.

We also provide the analytic fit formulas of absorption cross section of OH^- and O_2^-

$$\sigma_{\lambda}(OH) = \frac{(4.40 + 11.7\lambda) \times 10^{-22}}{1 + \exp[(\lambda/8.70 - 0.0774) \times 10^3]}, \quad \text{(B8)}$$

$$\sigma_{\nu}(O_2) = h\nu(h\nu - 0.46)^{3/2}\{0.70 - (h\nu - 0.46)[0.33$$
$$- 0.053(h\nu - 0.46)]\} \times 10^{-21}, \quad \text{(B9)}$$

where λ is in μm and $h\nu$ is in eV. Then the absorption coefficient is

$$\kappa_{\lambda,i} = \sigma_i n_i^-, \quad \text{(B10)}$$

where $i = OH^-, O_2^-$.

When all the absorption coefficients are clear, with formulas (15) and (16), we find that

$$P_{\lambda}(t) = 8\pi^2 \int_0^R \int_0^{2\sqrt{R^2-y^2}} n^2\kappa P_{\lambda}^{Pl} e^{-\kappa x} y\,dx\,dy. \quad \text{(B11)}$$

For the case of spherically symmetry, Planck radiation intensity $P_{\lambda}^{pl} = P_{\lambda}^{pl}[T(r)]$ is the function of the temperature and it is only r dependent, thus the absorption coefficient is also only r dependent. In this case (B11) may be simplified as

$$P_{\lambda}(t) = 8\pi^2 \int_0^R \int_{-1}^1 n^2\kappa(r)P_{\lambda}^{Pl}(r)e^{-\kappa[rx+\sqrt{R^2-r^2(1-x^2)}]}r^2\,dr\,dx. \quad \text{(B12)}$$

[1] D. F. Gaitan, L. A. Crum, C. C. Church, and R. Roy, J. Acoust. Soc. Am. **91**, 3166 (1992).

[2] B. P. Barber and S. J. Putterman, Nature (London) **352**, 318 (1991).

[3] D. J. Flannigan and K. S. Suslick, Nature (London) **434**, 52 (2005).

[4] R. A. Hiller, S. J. Putterman, and K. R. Weninger, Phys. Rev. Lett. **80**, 1090 (1998).

[5] B. Gompf, R. Gunther, G. Nick, R. Pecha, and W. Eisenmenger, Phys. Rev. Lett. **79**, 1405 (1997).

[6] M. J. Moran and D. Sweider, Phys. Rev. Lett. **80**, 4987 (1998).

[7] B. P. Barber *et al.*, Phys. Rep. **281**, 65 (1997).

[8] R. Hiller, S. J. Putterman, and B. P. Barber, Phys. Rev. Lett. **69**, 1182 (1992).

[9] P. T. Greenland, Contemp. Phys. **40**, 11 (1999).

[10] J. B. Young, J. A. Nelson, and W. Kang, Phys. Rev. Lett. **86**, 2673 (2001).

[11] M. P. Brenner, S. Hilgenfeldt, and D. Lohse, Rev. Mod. Phys. **74**, 425 (2002).

[12] S. Hilgenfeldt, S. Grossmann, and D. Lohse, Nature (London) **398**, 402 (1999).

[13] G. E. Vazquez and S. J. Putterman, Phys. Rev. Lett. **85**, 3037 (2000).

[14] B. D. Storey and A. J. Szeri, Proc. R. Soc. London **456**, 1685 (2000).

[15] Y. An, C. G. Xie, and C. F. Ying, Chin. Phys. Lett. **20**, 575 (2003).

[16] B. D. Storey and A. J. Szeri, Phys. Rev. Lett. **88**, 074301 (2002).

[17] Xie Chongguo, An Yu, and Ying Chongfu, Acta Phys. Sin. **52**, 102 (2003).

[18] C. F. Ying, Y. An, and C. G. Xie, J. Phys. D **38**, 2489 (2005).

[19] L. Yuan, Phys. Rev. E **72**, 046309 (2005).

[20] K. Yasui, Phys. Rev. E **64**, 016310 (2001).

[21] D. Hammer and L. Frommhold, Phys. Rev. E **65**, 046309 (2002).

[22] Y. An and C. F. Ying, Phys. Rev. E **71**, 036308 (2005).

[23] L. D. Landau and E. M. Lifshitz, *Statistical Physics* (Pergamon Press, New York, 1980), 2nd edition.

[24] L. Rayleigh, Philos. Mag. **34**, 94 (1917); M. Plesset, J. Appl. Mech. **16**, 277 (1949); B. Noltingk and E. Neppiras, Proc. Phys. Soc. London, Sect. B **63**, 674 (1950); J. B. Keller and I. I. Kolodner, J. Appl. Phys. **27**, 1152 (1956).

[25] T. Ishiyama, T. Yano, and S. Fujikawa, Phys. Fluids **16**, 4713 (2004).

[26] D. Lohse, M. P. Brenner, T. F. Dupont, S. Hilgenfeldt, and B. Johnston, Phys. Rev. Lett. **78**, 1359 (1997).

[27] S. Geltman, J. Quant. Spectrosc. Radiat. Transf. **13**, 601 (1973).

[28] L. M. Branscomb *et al.*, Phys. Rev. **111**, 504 (1958).

[29] S. J. Smith and D. S. Burch, Phys. Rev. Lett. **2**, 165 (1959).

[30] S. Geltman, Astrophys. J. **136**, 935 (1962).

[31] L. M. Branscomb, Phys. Rev. **148**, 11 (1966).

[32] D. S. Burch, S. J. Smith, and L. M. Branscomb, Phys. Rev. **112**, 171 (1958).

[33] D. Hammer and L. Frommhold, J. Mod. Opt. **48**, 239 (2001).

[34] W. C. Moss, D. A. Young, J. A. Harte, J. L. Levatin, B. F. Rozsnyai, G. B. Zimmerman, and I. H. Zimmerman, Phys.

Rev. E **59**, 2986 (1999).

[35] J. S. Dam and M. T. Levinsen, Phys. Rev. Lett. **92**, 144301 (2004).

[36] J. B. Keller and M. Miksis, J. Acoust. Soc. Am. **68**, 628 (1980).

[37] N. Xu, R. E. Apfel, A. Khong, X. Hu, and L. Wang, Phys. Rev.

E **68**, 016309 (2003).

[38] R. Toegel, S. Hilgenfeldt, and D. Lohse, Phys. Rev. Lett. **88**, 034301 (2002).

[39] Y. T. Didenko, W. B. McNamara III, and K. S. Suslick, Nature (London) **407**, 877 (2000).

[40] D. J. Flannigan and K. S. Suslick, ARLO **6**(3), 157 (2005).